



# On Ski–Snow Contact Mechanics During the Double Poling Cycle in Cross-Country Skiing

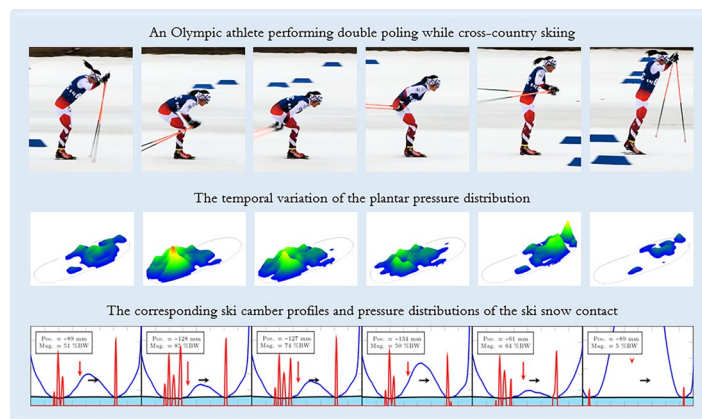
Gustav Hindér<sup>1</sup> · Kalle Kalliorinne<sup>1</sup> · Joakim Sandberg<sup>1</sup> · Andreas Almqvist<sup>1</sup> · Hans-Christer Holmberg<sup>2,3</sup> · Roland Larsson<sup>1</sup>

Received: 25 August 2023 / Accepted: 6 February 2024  
© The Author(s) 2024

## Abstract

Of the medals awarded during the Winter Olympics Games, most are awarded for sports involving cross-country (XC) skiing. The Double Poling (DP) technique, which is one of the sub-techniques used most frequently in XC skiing, has not yet been studied using simulations of the ski–snow contact mechanics. This work introduces a novel method for analysing how changes in the distribution of pressure on the sole of the foot (Plantar Pressure Distribution or PPD) during the DP motion affect the contact between the ski and the snow. The PPD recorded as the athlete performed DP, along with an Artificial Neural Network trained to predict the geometry of the ski (ski-camber profile), were used as input data for a solver based on the boundary element method, which models the interaction between the ski and the snow. This solver provides insights into how the area of contact and the distribution of pressure on the ski-snow interface change over time. The results reveal that variations in PPD, the type of ski, and the stiffness of the snow all have a significant impact on the contact between the ski and the snow. This information can be used to improve the Double Poling technique and make better choices of skis for specific snow conditions, ultimately leading to improved performance.

## Graphical Abstract



**Keywords** Cross-country skiing · Sports technology · Contact-mechanics · Plantar pressure · Ski-camber

✉ Gustav Hindér  
gustav.hinder@ltu.se

<sup>1</sup> Division of Machine Elements, Luleå University of Technology, Luleå, Sweden

<sup>2</sup> Division of Health, Medicine and Rehabilitation, Luleå University of Technology, Luleå, Sweden

<sup>3</sup> School of Kinesiology, University of British Columbia, Vancouver, BC, Canada

## Abbreviations

XC Cross-country  
DP Double poling  
PPD Plantar pressure distribution  
ANN Artificial neural network  
BEM Boundary element method  
BW Body weight

HBW	Half body weight
FBW	Full body weight
FS	Foot size
CH	Camber height
$E$	Young's Modulus MPa
$\nu$	Poisson's ratio

## 1 Introduction

At the Winter Olympics, the greatest overall number of awarded medals are in disciplines involving Cross-Country (XC) skiing. During the 2022 Games in Beijing, a 1 % improvement in the finishing times of 31 athletes who came in from second to eighth place would have enabled them to win a gold medal instead. The many ways in which performance can be improved include enhancing the physiological capacity of the athlete and selecting the appropriate pair for the skier and preparing them in a suitable manner for the prevailing weather and snow conditions.

Cross-country skiing is divided into two categories or techniques, skating or freestyle skiing, and classic skiing. Classic skiing is characterised by the combination of having grip wax in the middle of the ski, in between the two glide zones. By applying more weight onto one ski, the grip wax is pushed down into the snow to generate a propulsive force with the legs. When less weight is applied to the skis, the grip zone is lifted and only the glide zone is in contact with the snow. During skating, where the grip zone does not exist on the skis, only gliding motions are utilised and propulsive forces from the legs are generated by pushing away with the skis in a V-shape. With both techniques, the skis are selected to be appropriate for prevailing snow conditions. Breitschädel defined cold conditions as temperatures  $-3^{\circ}\text{C}$ , with new or partially transformed snow of low snow humidity, while under warm conditions, the transformed snow grains are wet and soft [1]. In the classic technique, one of the most important sub-techniques is double poling (DP), where the athlete holds her skis parallel and pointed in the direction of motion, while using only the poles and, in particular, the upper body for propulsion, not utilising the grip wax. Movements of the skier during the DP cycle cause distinctive changes in the plantar pressure distribution (PPD), including the load magnitude and position of the feet relative to the ski. For example, in their study of the biomechanics of DP performed by elite XC skiers, Holmberg et al. [2] found that the load is redistributed from the rearfoot to the forefoot during the recovery phase until the body is elevated and no load is applied on the ski. Whereas upon initiation of the poling phase, the load on the forefoot increases, followed by an increase in the load on the rearfoot until the cycle is finished. While Holmberg et al. [2] considered DP and presented the PPD divided into forefoot

and rearfoot, Pavalier [3] considered skating and presented the PPD divided into lateral and medial (outside and inside). To the best of our knowledge, no one has presented a high-resolution positioning of the centre of pressure for each foot during XC skiing.

Following this seminal work [2], many other researchers have studied various aspects of DP [4–14]. However, they have focused primarily on the generation of propulsive forces, while less focus has been given to the resistive forces in the DP cycle, which also exert a considerable impact on overall performance. These forces include the gravity working against the body in uphill sections, the air drag of the athlete's body, and the friction in the ski–snow interface. The latter one, which has been studied for many years, focuses primarily on static gliding without including the impact of dynamic body movements. Bowden and Hughes [15] performed an early study and investigated the friction between solid materials and ice. Their concluding suggestion was that the relatively low friction of objects sliding on ice and snow temperature below  $0^{\circ}\text{C}$ , occurs due to the generation of a lubricating water layer caused by friction melting, not pressure melting. Following this work, Bowden [16] alone conducted experiments using real skis, comparing materials, temperature, and hardness. Since then, several groups [17–20] have studied the subject and tried to connect ski–snow friction to the affecting mechanisms. For a summary of the major factors that influence ski–snow friction during XC skiing, see Colbeck [21] or Almqvist et al. [22].

In their review, Almqvist et al. [22] emphasised that the shape of the ski's camber profile and its respective front and rear contact zones, also called glide zones, have the biggest impact on the ski–snow friction. This justifies the many works trying to understand the contact mechanics of the ski–snow contact. The ski–snow contact can be described as a multi-scale problem including a micro-scale, considering the contact characteristics between individual snow grains and asperities on the ski-base structure, a meso-scale encompassing, e.g., ski-base's unevenness, and a macro-scale, including the apparent contact characteristics considering the contact as seen by the naked eye. However, since it is nearly impossible to analyse the ski–snow contact itself, there are many challenges in describing it. Nonetheless, there are many ways of simulating contact mechanics problems, see, e.g., [23, 24]. Mössner et al. [25] investigated the mechanical properties of snow and used the snow hardness and failure shear stress to simulate the ski–snow contact. Later, Mössner et al. [26] calculated the contact area between snow grains and ski-base using numerical methods. Similarly, Theile et al. [27] modelled the behaviour of snow of the ski–snow contact and calculated the relative real contact area to be 0.4 %. While the previously mentioned research has investigated what we call the real contact area, the apparent ski–snow contact area has also

been investigated. Bäckström et al. [28] developed a method to measure the pressure distribution of a full-length ski to characterise the contact and use the results to improve the ski selection for different conditions. With respect to choosing skis that are optimal for the conditions at hand, Breitschädel [29] examined the characteristics of a variety of male and female classical XC skis used by the Norwegian national team in an attempt to determine the key parameters for use in warm and cold conditions. In this context, he developed a model designed to approximate the apparent area of contact, defining contact as a distance less than 0.05 mm between the ski and the underlying surface. He found that in comparison to skis used under cold conditions, skis chosen for warmer conditions were, in general, stiffer, with a higher and shorter camber and shorter apparent contact area between both the front and back glide zones and the snow. Using a similar method, Kalliorinne et al. [30] presented the pronounced changes in the ski-camber profile and the ski-snow contact characteristics when shifting the applied load in magnitude and position when employing different tucking postures in the gliding position.

In recent years, there has been an increase in the usage of Artificial Neural Networks (ANN), to improve the accuracy and reduce the computational time of numerical simulations of tribological contact problems [31, 32]. With the foundation of these ideas, Kalliorinne et al. [33] developed a numerical method incorporating an ANN and a Boundary Element Method (BEM) contact mechanics solver to characterise the apparent ski-snow contact, including the apparent contact area and pressure.

The above-mentioned previous studies on the ski-snow contact have, to the best of our knowledge, mainly focused on skiers in a static position. Hence, the dynamic interplay between skier biomechanics and the ski-snow contact, during the DP cycle remains unexplored. Consequently, our investigation delves into the alterations in the overall (macro-scale) characteristics of the ski-snow contact among classical XC skis, for cold, universal, and warm conditions, and snow. We analyse these changes in response to shifts in the Plantar Pressure Distribution (PPD) during the DP cycle, adding a new dimension to our understanding.

## 2 Method

The method adopted herein is presented in the following subsections. It starts with a general overview in Sect. 2.1. Then, the double poling cycle is presented in Sect. 2.3 followed by a description of how the plantar pressure distribution (PPD) was obtained from the double poling (DP) tests in Sect. 2.4. In Sect. 2.5 the method employed to obtain the contact mechanics output based on the plantar pressure measurement data are presented.

### 2.1 General Overview

While double poling (DP) on snow in flat terrain at competition speed (ca 20 km/h), the PPD of a female Olympic gold medallist was recorded. Three pairs of classical XC skis made for cold, universal, and warm conditions, from now on denoted as the “cold”, “universal”, and “warm” ski, were prepared with wax and used in the test for six runs each. During each run, load magnitude and position calculated from PPD measured during eight subsequent DP cycles were used as input data for a contact mechanics solver. The ski-camber profiles of the three different skis were measured for pertinent load conditions (load magnitudes and positions). An ANN was trained to predict the shape of each ski in all possible loading conditions and was together with the PDD data used as input data in a script, simulating the macro-scale contact mechanics of the ski-snow interface at two different snow stiffness [33]. For each ski, the script simulated the ski-snow apparent contact length and pressure of the rear and front glide zones.

### 2.2 The Skis

Three pairs of classical XC skis, “cold”, “universal”, and “warm”, suitable for the athlete’s body weight (BW), were selected in consultation with a professional ski technician. All were the Speedmax model (Fischer Sports GmbH, Ried im Innkreis, Austria), with the model 902 camber, and the type 28 base material (an ultra-high molecular weight polyethylene-based polymer with unknown additives). In addition, all ski pairs had micro-structural base grinds suitable for the respective conditions under which they were to be used. Before testing, the base of all skis was treated with the same glide and grip wax on the glide and grip zones indicated by the ski technician.

The skis were characterised using a SkiSelector (SkiSelector Sportdata AB, Öjebyn, Sweden) to obtain fundamental data about the camber height, stiffness, and contact zones. The camber height at the balance point, under a load of half (HBW) and full (FBW) body weight, together with the lengths of the rear and front contact zones under HBW, when the load is applied 13 cm behind the balance point, are presented in Table 1. The camber height at the balance point, as a function of the load, applied 7 cm behind the balance point, is presented in Fig. 1. The balance point, designated as 0, is defined as the location along the ski where it can be balanced on a narrow support and is the location where the fastening point of the binding is positioned.

### 2.3 The Double Poling Cycle

The double poling (DP) cycle in XC skiing involves a poling and a recovery phase. This is illustrated in Fig. 2, by a

**Table 1** General characteristics of the “cold”, “universal”, and “warm” skis. Including camber height, under a load of HBW and FBW, and rear and front contact length under a load of HBW, when load is applied 13 cm behind the balance point

Ski	Camber Height [mm]		Contact Length [mm]	
	HBW	FBW	Rear	Front
Cold	1.15	0.32	210	157
Universal	1.34	0.30	183	132
Warm	1.48	0.29	143	83

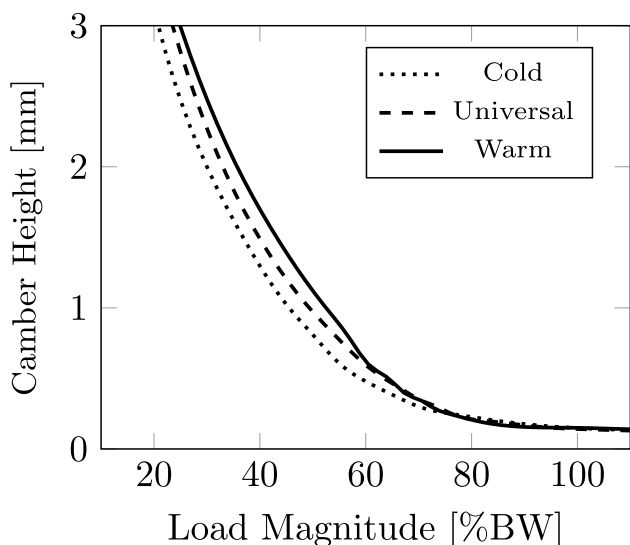


**Fig. 1** Camber height as a function of the load applied 7 cm behind the balance point of the “cold” (dotted curve), “universal” (dashed curve), and “warm” (solid curve) skis

sequence of 6 intermediate steps explained as follows. The poling phase is initiated by the activation of the core muscles and a slight hip flexion, followed by the planting of the poles into the snow (1). As the upper body continues to

lean forward and the hip flexion increases (2), more BW is loaded onto the poles and snow, thereby generating propulsion. During this poling phase, the boots are gradually flattened onto the ski, increasing the load while redistributing it from the front towards the rear of the foot. This phase ends with the arms extended, poles pointing backwards, and the BW loaded mostly on the heel (3). The subsequent recovery phase then starts with raising the upper body while continuing to glide in the direction of travel (4). At the same time, the arms move forward, the body is extended, and the load on the foot is moved forward as the athlete pushes off (5). Finally, the arms are positioned to begin a new cycle, with the body being elevated with a slight forward lean, usually with no load on the foot (6).

## 2.4 Plantar Pressure Distribution Measurements

The Plantar pressure distribution (PPD) was measured using Medilogic wireless insoles (T & T medilogic Medizintechnik GmbH, Schönefeld, Germany) of suitable size, inserted into a pair of XC ski boots chosen by the athlete, and recorded with Medilogic Pressure Measurement software through WiFi transmission, with a sampling frequency of 100 Hz. The soles used were of the size 36/37, including 107 (15 × 7.5 mm) surface resistive solid state relay sensors (measuring up to 100 N/cm<sup>2</sup> with a measuring error of ±5%), distributed over the whole insole, resulting in an insole length of 240 mm. The load magnitude is calculated as the sum of all sensors’ pressure values divided by their total area and the load position is calculated as the resulting centre of pressure along the coronal plane using moment equilibrium. The load magnitude was calibrated with respect to the athlete’s BW and a filter was adapted to compensate data for sensor drift (a slight increase of load magnitude over time due to sensor degradation). The PPD during each of the 6 steps of one DP cycle (presented in Fig. 2) is visualised in Fig. 3 where the heel is to the left and the toes are to the right.

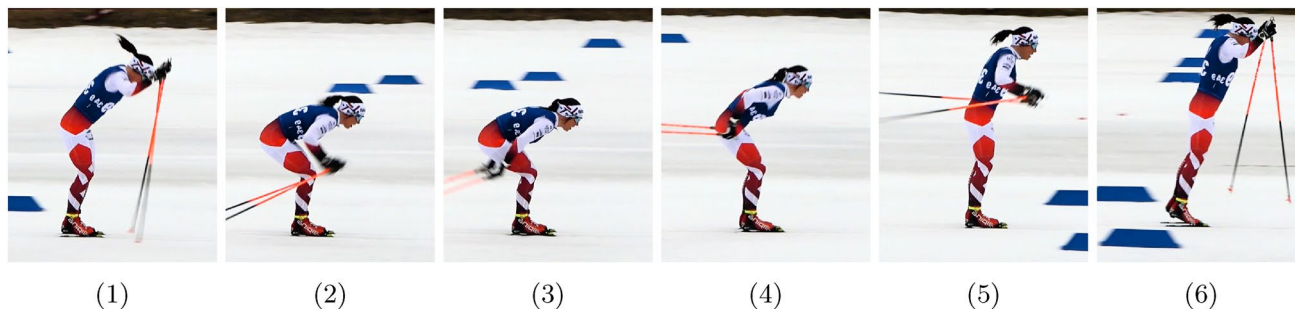


**Fig. 2** Visualisation of six steps of the DP sub-technique including (1) pole plant/start poling phase, (2) poling, (3) end of poling phase/start of the recovery phase, (4) recovery phase, (5) toe pushoff, (6) flight phase

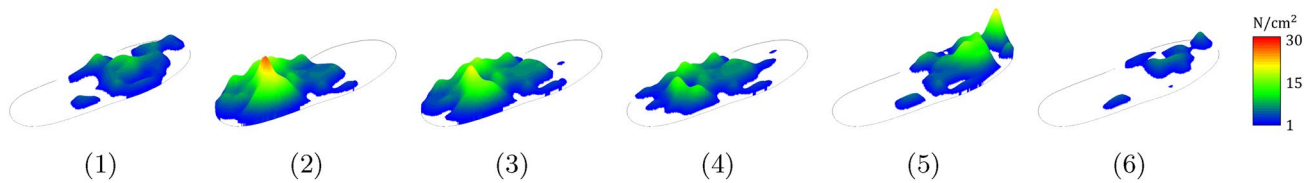


**Fig. 3** The PPD of the athlete's right foot during the 6 steps of the DP cycle depicted in Fig. 2. The pressure is visualised as a colour-coded topographical surface according to the colour bar on the right. In each figure the heel is to the left and the toes towards the right

In previous research, the planting of the poles has been used to determine the cycle start [2, 6, 34–36]. However, in the present study, considering the ski–snow contact, it is more applicable to determine the initiation of the cycle as the time when the ski begins to take load after the flight phase (corresponding to the PPD in (6) in Fig. 2), i.e., where the load exhibits minimum values. Consequently, the PPD of the right and the left foot from 8 consecutive cycles from each of the 6 runs for each ski pair were split at the start of a new cycle, where the load magnitude reaches its minimum value. This resulted in a data set of 48 cycles per foot and ski pair (“cold”, “universal”, “warm”). The PPD data for each foot were then combined and normalised to the skier's BW and a representative PPD was obtained by averaging over the 48 cycles per ski pair. Hereafter, the PPD data were incorporated into the contact mechanics analysis.

## 2.5 Contact Mechanics Analysis

For the contact mechanics analysis, the methodology presented by Kalliorinne [33] was adapted for temporal measurements and used in the present work. In addition to measurements on the macro-scale, this approach involves the determination of the ski-base unevenness on the meso-scale, i.e., a scale intermediate to the macro- and micro-scale (which could all be considered in the multi-scale problematic of the ski-snow contact [37]), with camber height between approximately a tenth of a millimetre down to a tenth of a micrometre [33, 38]. These temporal measurements provide values utilised for predicting ski-camber profile deformation, along with calculating ski-snow contact pressure and length. Measurements of the ski-camber profile of one ski of each ski pair (“cold”, “universal”, and “warm”) for the pertinent range of loading conditions, with a 5 kg increment for load magnitude and a 3 cm increment in load position, were done using a SkiSelector. The SkiSelector uses a stylus apparatus to measure the vertical displacement (with a resolution of about 0.01 mm) of the ski along a 2D profile approximately 2000 mm long (with a resolution of about 1 mm) at a sampling rate of 200 Hz. The load is applied through a measurement boot (of size corresponding to the athlete's boot), attached at the

boot–ski connection point located at the toes of the boot and the middle of the ski. An Artificial Neural Network (ANN) of each ski was trained with the corresponding ski-camber profile data. Furthermore, the load conditions, the ANN, and a Matlab (Mathworks, Massachusetts, United States) script based on the Boundary Element Method (BEM) described in [39], with the elastoplastic approximation described in [40], were used for the analysis of the contact mechanics. The BEM model is based on a model for two semi-infinite half-spaces in contact (assuming that the contact pressure along the 44 mm wide ski is uniform) under a plain strain condition. In this case, the contact is considered to occur between one perfectly flat linear-elastic body, with Young's modulus equivalent to the snow and the ski-base combined, and one rigid body taking the geometry of the ski-camber profile, as predicted by the ANN for a given loading condition. The output of the simulation is the apparent contact pressure and length of the front and rear contact zone of the ski. The apparent contact length (rather than area since the simulation is made as a 2D line of the ski-camber) is described as the length of the zones along the sliding direction where contact between ski and snow occurs, defined as the apparent contact pressure being greater than zero. For the two simulations, the snow was considered to have Young's modulus  $E_{\text{snow}} = 50$  MPa and  $E_{\text{snow}} = 200$  MPa, respectively, and the ski-base material  $E_{\text{ski}} = 900$  MPa. The Poisson ratio was specified as  $\nu = 0.3$  for both the snow and the ski-base material. This represents a soft- and a medium-stiff case, as compacted snow in a ski track or similarly has been observed to have Young's moduli in the range of 20 to 400 MPa [41–43].

## 3 Results and Discussion

The averaged load magnitude (red solid curve, in % of the skier's BW) and position (relative to the boot–ski connection point)(blue dotted curve, in mm), with the standard deviation as the shaded areas (68 % confidence interval), of one foot calculated from all cycles for each one of the skis (“cold”, “universal”, and “warm”) are depicted as temporal functions

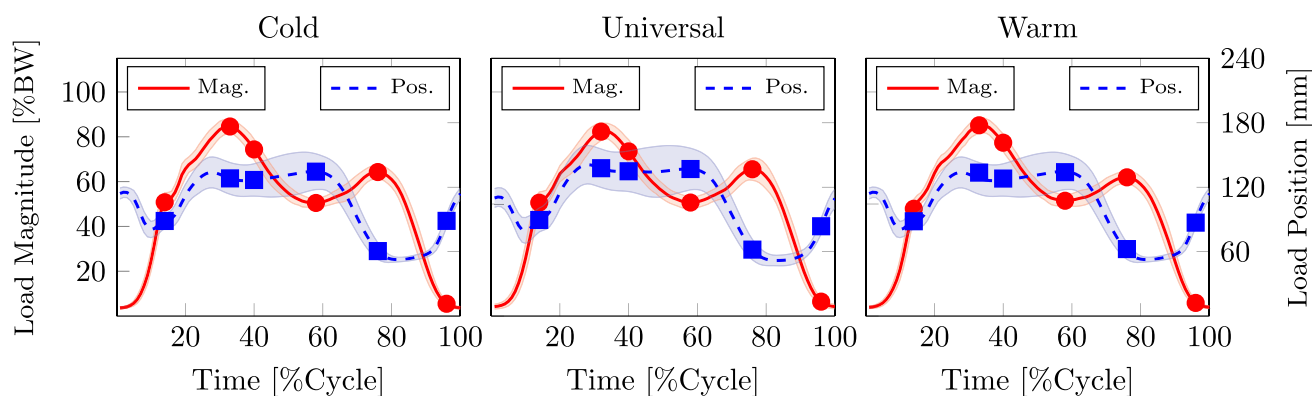


**Fig. 4** Averaged load magnitude (red/solid line) and load position (blue/dashed line) with corresponding standard deviation (shaded area) calculated from the retrieved PPD of the DP cycles on each pair

(in % of cycle time) in Fig. 4. Dot (load) and square (position) markers indicate the six steps of the DP cycle from Fig. 2.

As seen by the temporal variation of the load magnitude and position, in Fig. 4, there are some minor but visual differences between the three pairs of skis. However, the general behaviour is the same. Step (1) in the investigation, is characterised by a distortion in the load curve due to the skier’s action of putting load into the poles as they are grounded in the snow. As seen by the input values, the load is around 50 % (on each ski) of the skier’s body weight at a position on the front of the foot. Step (2) is when the highest load is applied during the cycle, caused by the movement of the body’s centre of gravity. Up to 85 % of the skier’s body weight, at a position towards the rear of the foot. In Step (3), the body is similarly positioned as in Step (2), but the load has started to decrease to 76 % of the body weight. Step (4) is in the middle of the recovery phase of the cycle where the load is approximately 50 % of the body weight towards the rear of the foot. Step (5) is at the end of the recovery phase when the skier pushes off from the ground to get the body into position for the next poling cycle. This gives rise to a load of around 65 % of the skier’s body weight placed on the forefoot. In Step (6) of the cycle, the flight phase, the skier has completely left the ground and the skis are barely in touch with the snow surface.

From the contact mechanics simulations, using the PPD data seen in Fig. 4, visualisations of the resulting ski-camber profiles (blue line), apparent contact areas and pressures (red line) for the three ski pairs (“cold”, “universal”, and “warm”) at the six investigated cycle steps are presented in Figs. 5 and 6, for the respective snow stiffness of  $E_{\text{snow}} = 50 \text{ MPa}$  and  $E_{\text{snow}} = 200 \text{ MPa}$ . The red arrow and the box denote the load magnitude and position, whereas the black arrow indicates the direction of travel. The black line visualises the deformed snow surface on top of the bulk snow visualised as the cyan fill.

of skis (“cold”, “universal”, and “warm”). The red circles and the blue dots display the six steps of the DP cycle, i.e., (1), (2), (4), (5), and (6) in Fig. 2 (Color figure online)

Figures 7, 8, and 9 depict a more detailed view of the apparent contact load (in % of the skier’s BW) (red curves, upper figures), and the corresponding apparent contact pressure (red curve, in kPa) and length (blue curve, in mm) (lower figures) of the rear (left column) and front (right column) glide zones, as a temporal function (in % of cycle time), calculated from all cycles of one foot for each one of the skis (“cold”, “universal”, and “warm”), respectively. The solid lines represent the simulations using  $E_{\text{snow}} = 50 \text{ MPa}$ , whereas the dashed line using  $E_{\text{snow}} = 200 \text{ MPa}$ . Dot (load and pressure) and square (length) markers indicate the 6 steps of the DP cycle from Fig. 2. For the six investigated cycle steps, the instantaneous apparent contact load, length, and pressure of the rear and front contact of the three different skis are presented in Table. 2 and 3 for the respective Young’s modulus.

For the three different ski pairs, the most pronounced differences in contact behaviour can be seen in Figs. 5 and 6. The skis used for cold conditions are characterised by a long rear contact zone and a low gap height at the balance point (0 dm), in comparison to the skis used for warm conditions where the contact zone is shorter, and the gap height is higher. These characteristics are connected to the characteristics of the ski–snow contact required at the given conditions, as well as the characteristics of the applied grip wax.

Looking at the “warm” ski, at both the soft and stiffer snow conditions, the rear contact zone is substantially shorter than for the “universal” and the “cold” ski, which can also be seen in more detail in Figs. 7, 8, and 9, as well as in Tables 2 and 3. This type of characteristic is probably required in snow conditions where the humidity is high in both air and snow, causing the risk of excessive water in the contact to increase the amount and size of capillary bridges [21, 43]. This increase could enhance the force required to break the capillary forces holding the water meniscus together and thereby elevate the overall friction force [21, 22, 43]. The use of a shorter contact zone would lessen this

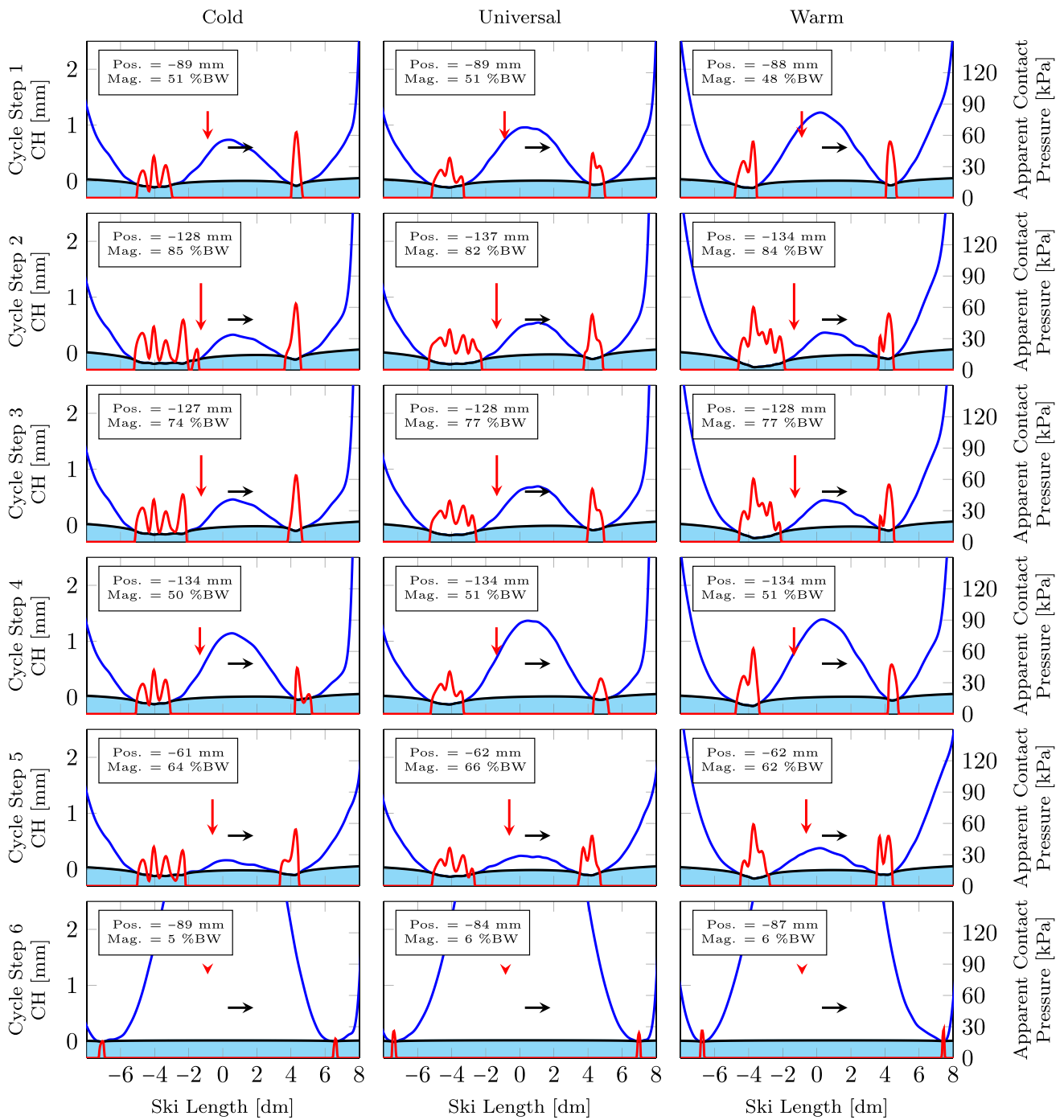


**Fig. 5** Resulting ski-camber profile (blue line) (measured as camber height (CH)), the deformed snow surface (black line and cyan fill), and the apparent contact area and pressure profile (red line) of the three skis (cold, universal, warm) at the six steps of the DP cycle, corresponding to the PPDs from the steps (1–6) in Fig. 2. The red arrow and the label box indicate the loading conditions. The horizontal position of the red

arrow indicates the load position and its length indicates the load magnitude. Correspondingly, the box label includes the load position measured from the balance point on the ski and the load magnitude on one ski as a percentage of the skier’s body weight. The black arrow indicates the ski’s direction of travel. The Young’s-modulus and Poisson’s ratio of the snow are set to 50 MPa and 0.3, respectively (Color figure online)

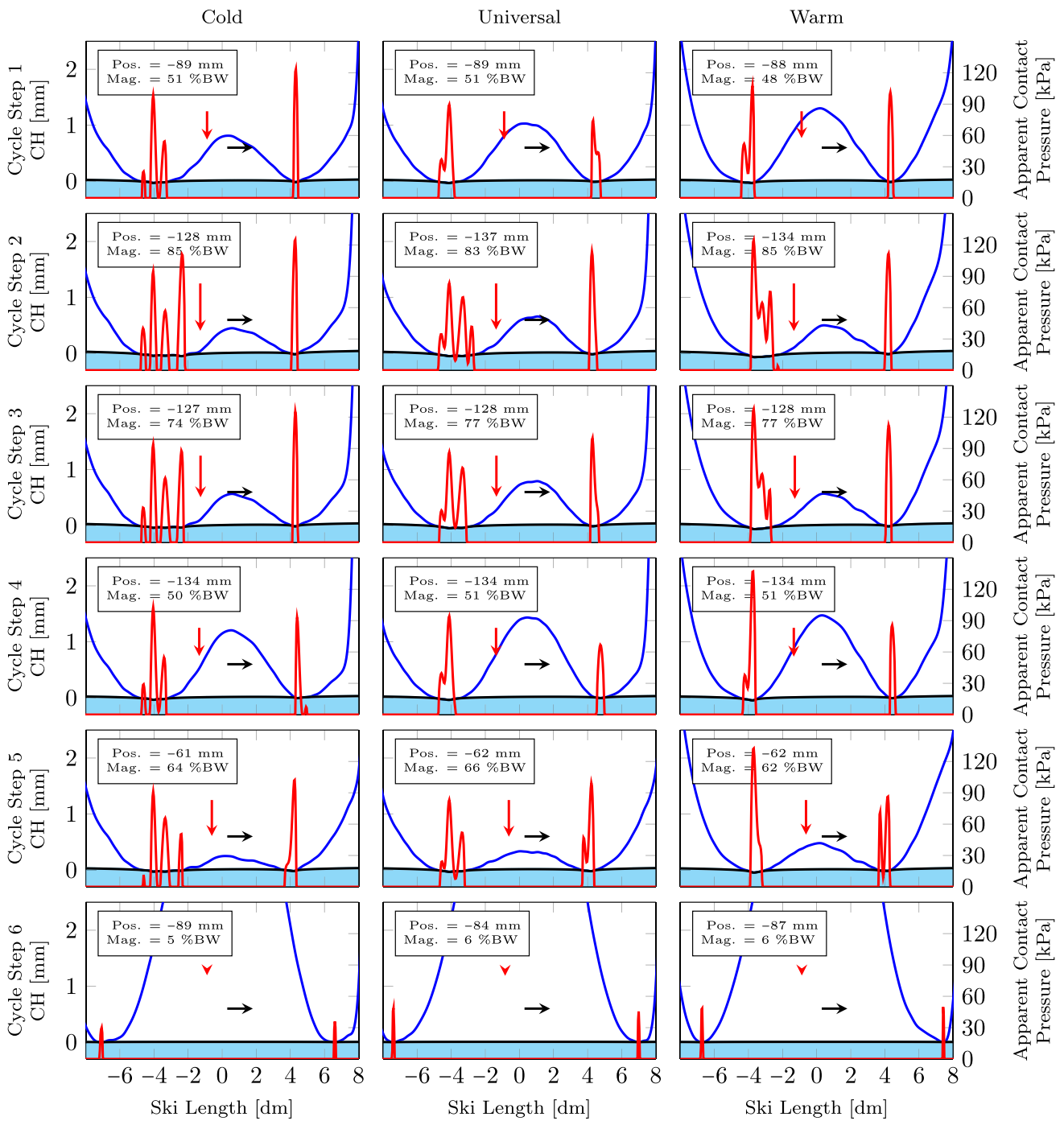


**Fig. 6** Resulting ski-camber profile (blue line)(measured as camber height (CH)), the deformed snow surface (black line and cyan fill), and the apparent contact area and pressure profile (red line) of the three skis (cold, universal, warm) at the six steps of the DP cycle, corresponding to the PPDs from the steps (1–6) in Fig. 2. The red arrow and the label box indicate the loading conditions. The horizontal position of the red

arrow indicates the load position and its length indicates the load magnitude. Correspondingly, the box label includes the load position measured from the balance point on the ski and the load magnitude on one ski as a percentage of the skier’s body weight. The black arrow indicates the ski’s direction of travel. The Young’s-modulus and Poisson’s ratio of the snow are set to 200 MPa and 0.3, respectively (Color figure online)



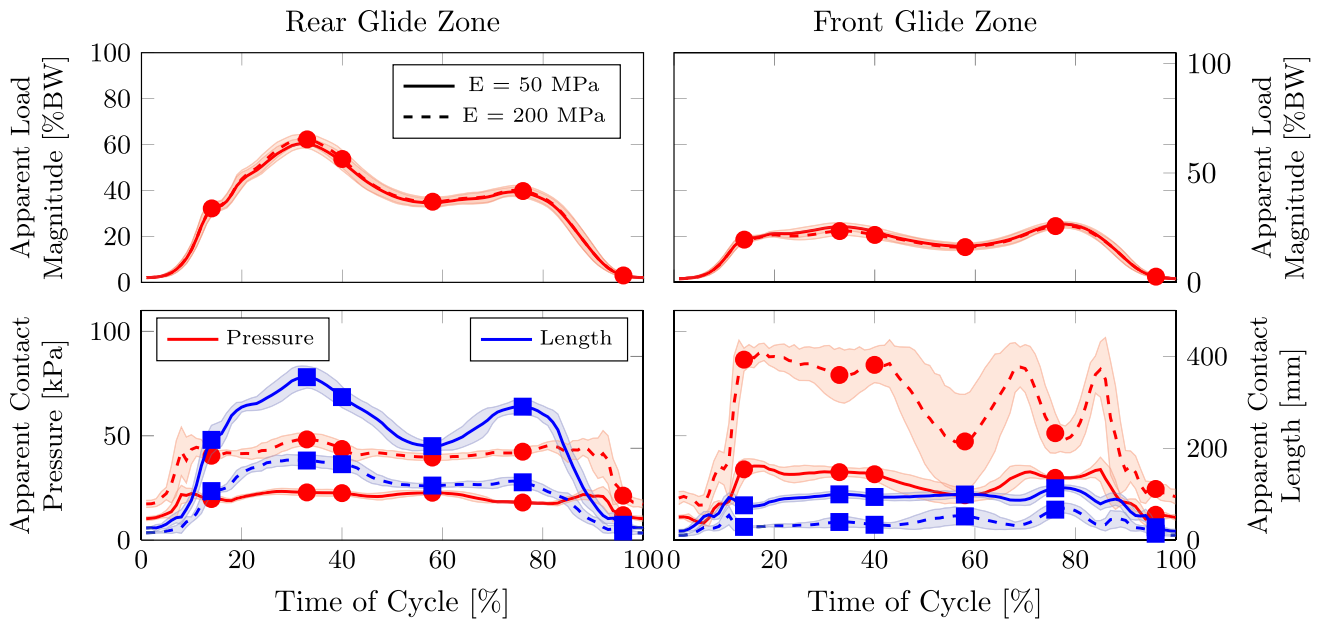


**Fig. 7** Cold ski. Mean (solid and dashed curves) and standard deviation (shaded areas, 68% confidence interval) of the apparent contact load (red curves, upper figures), pressure (red curves, lower figures) and length (blue curves, lower figures) of the rear (left figures) and

front (right figures) glide zones, for the simulation on snow with  $E_{\text{snow}} = 50$  MPa (solid curves) and  $E_{\text{snow}} = 200$  MPa (dashed curves). Red dots (contact load and pressure) and blue squares (contact length) denote the cycle steps (Color figure online)

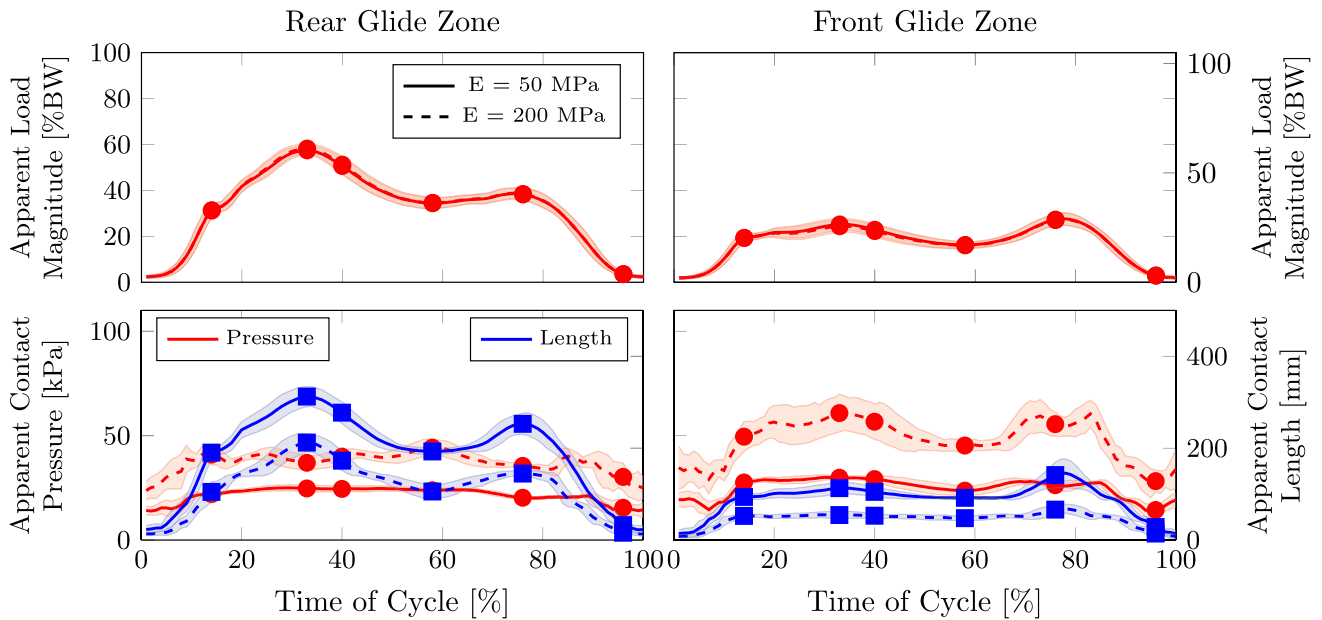


**Fig. 8** Universal ski. Mean (solid and dashed curves) and standard deviation (shaded areas, 68% confidence interval) of the apparent contact load (red curves, upper figures), pressure (red curves, lower figures) and length (blue curves, lower figures) of the rear (left fig-

ures) and front (right figures) glide zones, for the simulation on snow with  $E_{\text{snow}} = 50$  MPa (solid curves) and  $E_{\text{snow}} = 200$  MPa (dashed curves). Red dots (contact load and pressure) and blue squares (contact length) denote the cycle steps (Color figure online)

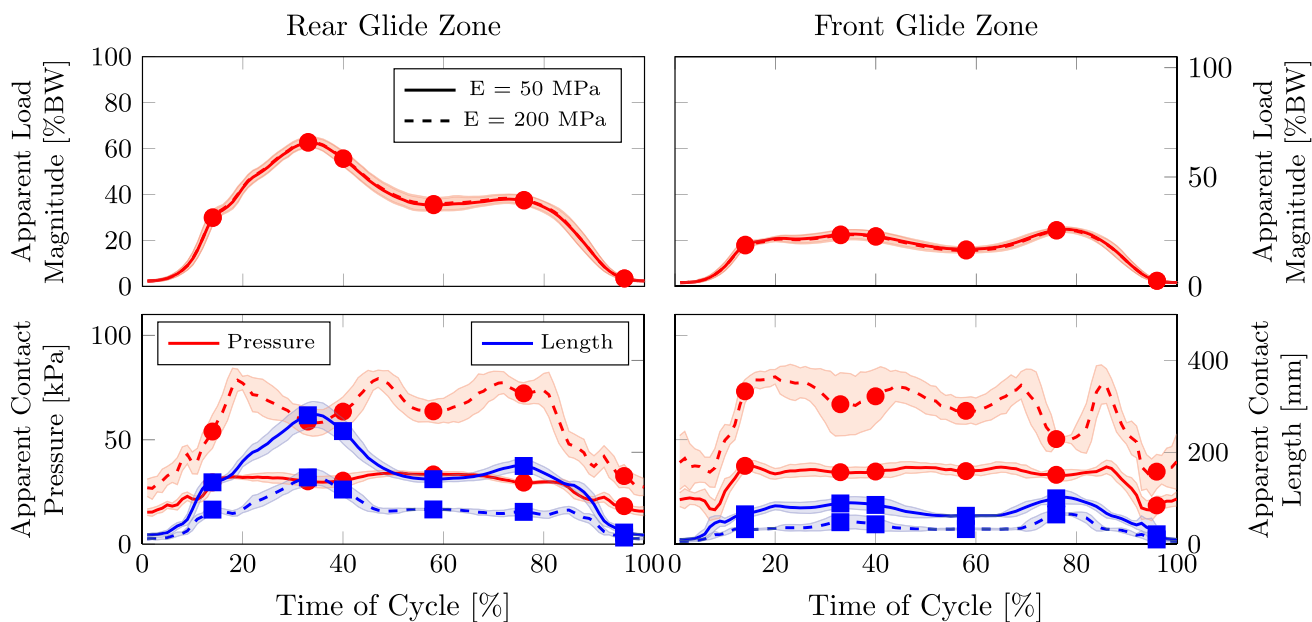


**Fig. 9** Warm ski. Mean (solid and dashed curves) and standard deviation (shaded areas, 68% confidence interval) of the apparent contact load (red curves, upper figures), pressure (red curves, lower figures) and length (blue curves, lower figures) of the rear (left figures) and

front (right figures) glide zones, for the simulation on snow with  $E_{\text{snow}} = 50 \text{ MPa}$  (solid curves) and  $E_{\text{snow}} = 200 \text{ MPa}$  (dashed curves). Red dots (contact load and pressure) and blue squares (contact length) denote the cycle steps (Color figure online)

**Table 2** Apparent contact load, pressure and length of the rear and front contact zone of the three classic skis (cold, universal, warm) at the four investigated steps of the DP cycle

Ski	Cycle step	Rear contact			Front contact		
		Load [%BW]	Pressure [kPa]	Length [mm]	Load [%BW]	Pressure [kPa]	Length [mm]
Cold	1	31.9	19.7	218	18.9	33.9	76
	2	60.4	22.9	355	24.2	32.6	100
	3	52.3	22.5	311	22.1	31.6	94
	4	34.7	22.7	205	15.8	21.5	99
	5	39.1	18.0	291	25.2	29.8	113
	6	3.0	11.9	34	2.5	12.2	28
Universal	1	31.3	21.9	190	19.3	27.6	94
	2	57.4	24.7	312	25.2	29.9	113
	3	50.6	24.5	277	22.9	29.2	105
	4	34.4	23.9	193	16.3	23.7	92
	5	38.2	20.3	253	27.3	26.3	142
	6	3.5	15.5	33	2.9	14.4	28
Warm	1	29.7	29.6	135	18.1	37.5	65
	2	62.5	30.1	281	22.6	34.5	89
	3	55.5	30.4	246	21.9	34.8	85
	4	35.3	33.4	141	16.1	35.0	62
	5	37.4	29.5	170	24.5	33.2	100
	6	3.4	18.2	25	2.4	18.5	22

**Table 3** Apparent contact load, pressure and length of the rear and front contact zone of the three classic skis (cold, universal, warm) at the four investigated steps of the DP cycle

Ski	Cycle step	Rear contact			Front contact		
		Load [%BW]	Pressure [kPa]	Length [mm]	Load [%BW]	Pressure [kPa]	Length [mm]
Cold	1	32.2	40.4	107	18.6	86.5	29
	2	62.3	48.3	173	22.3	79.1	40
	3	53.7	43.7	165	20.6	83.9	34
	4	35.1	39.6	119	15.4	47.3	52
	5	39.8	42.4	126	24.5	51.2	66
	6	3.0	21.3	19	2.5	24.5	14
Universal	1	31.3	40.9	105	19.3	49.5	53
	2	58.2	37.0	212	24.4	60.8	55
	3	51.2	40.0	173	22.3	56.7	53
	4	34.6	44.3	106	16.1	45.3	48
	5	38.4	35.5	145	27.1	55.5	66
	6	3.5	30.2	16	2.9	28.2	14
Warm	1	30.1	53.9	75	17.8	73.2	33
	2	62.9	58.7	145	22.3	67.0	48
	3	55.7	63.5	119	21.6	70.8	43
	4	35.9	63.6	76	15.6	63.9	33
	5	37.6	72.2	70	24.3	50.3	65
	6	3.5	32.6	14	2.4	34.7	10

effect. Also, important to notice is the camber behaviour, a high camber with a sharper entrance and exit of the contact will lower the amount of water meniscus and ease the breakage of the same [22]. On the contrary, both the “cold” and the “universal” skis have a much longer rear contact zone. As the temperature drops, the humidity and the possible water in the contact decreases, lowering the need for a short contact.

It should be noted that the water capillary (or water shearing) hypothesis is debated. For example, Lever et al. [44] propose a mechanism based on snow abrasion, while questioning the melting theory by showing that melting may not occur at all under relatively low temperatures. However, in our opinion, it is unclear, how the abrasion will vary with the size of the contact patches, hence, we plan to investigate this phenomenon in coming studies. Still, a low contact area is important to minimise other friction mechanisms such as adhesion and micro-ploughing, but this is rather adjusted on the micro-scale grind on the ski-base surface [22].

During most of the cycle steps, for all skis and under both conditions of snow stiffness, the rear contact pressure, depicted in Figs. 5 and 6, demonstrates an undulating pattern. This pattern is related to the unevenness of the ski-base surface on the meso-scale. For the simulation with stiffer snow, the peak pressures are more pronounced compared to softer snow, where the pressure is more evenly distributed across the area of contact. This can be a way to lower the real area of contact, especially when the snow is stiff, which

might help in reducing the amount of wetted area, while distributing the contact pressure over a relatively large area, in order to minimise deformation of the snow.

The usage of a linear-elastic model for contact mechanics analysis is a debatable matter. The model of Almqvist et al. [39] was developed primarily for a metal-metal contact where both materials are known to have linear-elastic behaviours and can without a doubt be considered as two half-spaces. In a recent review by Surkutwar et al. [45], multiple material models including linear-elastic, elastic-plastic, and elastic-visco-plastic, were presented to be in use, all with good approximation. However, a ski with a thin layer ( $\approx 1$  mm) of polyethylene on a glass/carbon-fibre surface surrounding a core of foam or a wooden honeycomb structure, most likely has a somewhat different behaviour. Also, the snow is in some sense more complex than a metal, mainly due to its many different types of grains and its ability to sinter over time. However, the action of grooming and compacting the snow before a ski race improves the mechanical properties of snow substantially. Intuitively, denser snow, as in a compacted XC ski track, should behave more like a linear-elastic material than porous snow, since the snow grains are more closely connected. Hence, a linear-elastic model for the ski-snow contact in a compacted classic ski track should be a good approximation.

Let us consider the numerical data of some snow properties. Untreated fresh snow can have a density below  $100 \text{ kg/m}^3$ , whereas the density of compacted snow can rise up to

900 kg/m<sup>3</sup>, as it turns into ice [41]. For a ski track, the density would be in the range of 400–600 kg/m<sup>3</sup> [25, 41]. Due to these differences, Young's modulus can range between 0.5 to 1000 MPa [41], and as previously mentioned, a ski track would fall between 20 to 350 MPa [33, 41, 42, 46], depending on conditions and compaction rate. For the simulations, two Young's moduli within this span were used.  $E_{\text{snow}} = 50$  MPa corresponds to freshly fallen snow with less compaction or snow above zero where wetting causes grains to separate.  $E_{\text{snow}} = 200$  MPa corresponds to a more compact snow surface at either cold temperatures where time has been allowing grains to sinter or close below zero where compaction and sintering occur faster. These differences in stiffness have a great impact on the final results, both in apparent contact length and pressure. A pronounced difference between the two cases is that the high stiffness case causes the contact length to stay relatively constant which induces pressure to fluctuate during the various loading of the cycle. Whereas for the less stiff case, the contact length has much more fluctuation and the pressure stays more constant. This is explained by the elastic deformation of the snow, resulting in more of the surface of the ski carrying the load when the stiffness is low in comparison to the stiff case where only a few contact spots are maintained. This behaviour is especially pronounced in the "cold" ski, where the pressure peaks of the rear contact are connected at a low snow stiffness, see Fig. 5, but separated at a high snow stiffness, see Fig. 6. These irregularities in the ski-base causing these pressure peaks are an effect of the macro-scale geometry of the ski. Perhaps an imperfection originating from the manufacturing process or a deliberate shape with beneficial properties that may have been discovered from large numbers of tests.

Regarding the possibility of deforming the snow during skiing, we need to consider its compressive strength. As for Young's modulus, the strength also increases with density, from around 0.1 kPa for fresh snow up to 10 MPa for ice. A compacted ski track would have around 100 kPa to 2 MPa [41]. Considering the pressure data obtained in our analysis there would be occurrences where the compressive strength could be reached. As seen in some of the spikes, a contact pressure of up to 60 kPa when  $E_{\text{snow}} = 50$  MPa and up to 140 kPa when  $E_{\text{snow}} = 200$  MPa. Considering that the contact pressure increases with snow stiffness, the compressive strength would also increase, making it unlikely for the snow in a classic ski track to deform if it has had time to sinter. Also, important to note is that much of the data in the literature is from bulk testing [41, 42], whereas the surface behaviour might differ.

Considering the body position of Steps (3) and (4) in Fig. 2 it is hard to believe there would be a pronounced difference in PPD, but the load condition data in Figs. 4, 5, and 6 indicates else. In Step (3), the load position is relatively

centred (at 127 of 240 mm), whereas in Step (4), it has moved backwards again, even though the athlete is rising to move the body forward. This can be explained by the skier intentionally pushing the toes upwards to lift the midpoint of the ski (0 dm). This will reduce the risk of grip wax touching the snow and increasing friction. As seen in Steps (3) and (4) in Fig. 5, the camber is somewhat deformed at the balance point, but the thin wax layer (100–500  $\mu\text{m}$ ) would still not be close to the snow. In the following Step (5), the body has been shifted forward and the skier is pushing off with the toes, which is clearly seen in the corresponding step in Fig. 5 of the corresponding step, the camber has been deformed almost completely, severely increasing the risk of grip wax touching the snow surface and causing friction to increase. However, there are some differences between the ski pairs. Especially seen in Step (5), the camber height is higher for the warmer skis since a thicker layer of grip wax is usually applied in those conditions. Also, the need for less contact with the snow and a faster angle increase to break the water bridges and meniscus, are deciding factors. As the movements of the skier are discussed in this section, it is important to note that these simulations try to mimic a dynamic motion with a static solution. In double poling, the ski is in constant motion in the skiing direction as the load is applied on top of it, whereas in the simulation, it is statically pressed against the snow with no forward motion.

## 4 Conclusions

We developed a method to simulate the ski–snow contact mechanics behaviour during a Double Poling (DP) cycle. The method includes measuring a skier's temporal variations in Plantar Pressure Distribution (PPD) with pressure-measuring insoles, obtaining the temporal variation of the loading conditions on the ski throughout the DP cycle. Furthermore, an Artificial Neural Network (ANN) of the investigated skis was constructed by measuring the ski-camber profile at several loading conditions using a macro-scale stylus. This ANN, in combination with the loading conditions and properties of the virtual snow counter surface, were used as input in a contact mechanics solver based on the Boundary Element Method (BEM). The solver's output is the apparent contact pressure and area of the ski–snow contact. Combining the time-resolved load magnitude and position from the whole cycle and the temporal variation of the ski-camber profiles, the solver provides the apparent contact pressures and areas of the ski–snow contacts throughout the DP cycle.

From the investigation conducted herein, we conclude that:

1. The PPD fluctuates somewhat within and between cycles of DP and depends on whether skis designed for cold, universal, or warm conditions are utilised. The impact of these differences on the ski-camber profile and the resulting apparent contact pressure and length requires further investigation.
2. The greatest load is applied during the second step of the DP cycle, at the rear of the foot, causing most of the load to be carried by the rear zone. Interestingly, during the fifth step, the load is positioned at the front of the foot, increasing the load on the front contact zone and deforming the ski considerably more than during the rest of the cycle.
3. The ski for warm conditions exhibits, in general, the smallest total contact area and thereby the highest contact pressure.
4. The ski for cold conditions demonstrates, in general, the longest contact and therefore the lowest contact pressure, spreading out the load over a larger area in softer snow.
5. The apparent contact pressure and area in the ski–snow contact are strongly connected to the stiffness, i.e., Young's modulus, of the snow. Greater stiffness entails higher contact pressure, with pronounced peaks and with a small contact area. In contrast, with lower stiffness, the snow will deform and spread the load over a bigger area, resulting in lower pressure. Consequently, on stiff snow, the average pressure fluctuates during the DP cycle while the total contact length is stable, whereas on soft snow, the total contact length fluctuates more, and the average pressure is more stable.

**Acknowledgements** The authors would like to acknowledge the support from the Swedish Olympic Committee and the Swedish Research Council. We would like to thank Glenn Robarth and his team at Kultur- och Fritidsförvaltningen, Luleå Kommun for preparing the ski tracks, and Prof. Ulrik Röijezon and Johan Jirlén at the Department of Health, Education, and Technology, Luleå University of Technology, for helping us setting up the Medilogic insole system for measurements.

**Author Contributions** All authors contributed to the conceptualisation, design and methodology of the study. GH, AA, and KK developed the software. G.H. collected the data, performed the analysis and wrote the original draft. All authors reviewed and commented on previous versions of the manuscript. All authors read and approved the final manuscript.

**Funding** Open access funding provided by Lulea University of Technology. This research was partly founded by the Swedish Olympic Committee and the Swedish Research Council: DNR 2019-04293.

**Data Availability** The research data will be made available upon request.

## Declarations

**Conflicts of interest** All authors declare no conflict of interest.

**Open Access** This article is licensed under a Creative Commons Attribution 4.0 International License, which permits use, sharing, adaptation,

distribution and reproduction in any medium or format, as long as you give appropriate credit to the original author(s) and the source, provide a link to the Creative Commons licence, and indicate if changes were made. The images or other third party material in this article are included in the article's Creative Commons licence, unless indicated otherwise in a credit line to the material. If material is not included in the article's Creative Commons licence and your intended use is not permitted by statutory regulation or exceeds the permitted use, you will need to obtain permission directly from the copyright holder. To view a copy of this licence, visit <http://creativecommons.org/licenses/by/4.0/>.

## References

1. Breitschädel, F.: Variation of Nordic classic ski characteristics from Norwegian national team athletes. *Proc. Eng.* **34**, 391–396 (2012). <https://doi.org/10.1016/j.proeng.2012.04.067>
2. Holmberg, H.-C., Lindinger, S., Stöggl, T.L., Eitzlmair, E., Müller, E.: Biomechanical analysis of double poling in elite cross-country skiers. *Med. Sci. Sports Exerc.* **37**(5), 807–818 (2005). <https://doi.org/10.1249/01.MSS.0000162615.47763.C8>
3. Pavailler, S., Hintzy, F., Millet, G.Y., Horvais, N., Samozino, P.: Glide time relates to mediolateral plantar pressure distribution rather than ski edging in ski skating. *Front. Sports Act. Living* **2**, 117 (2020). <https://doi.org/10.3389/fspor.2020.00117>
4. Canclini, A., Baroni, G., Lindinger, S., Pozzo, R.: Mechanical energy and kinematics of double poling technique performed at different inclines by world-level cross-country skiers during world cup races. *J. Sci. Sport Exerc.* **3**, 270–280 (2021). <https://doi.org/10.1007/s42978-021-00128-y>
5. Carlsson, T., Fjordell, W., Wedholm, L., Swarén, M., Carlsson, M.: The modern double-poling technique is not more energy efficient than the old-fashioned double-poling technique at a sub-maximal work intensity. *Front. Sports Act. Living* (2022). <https://doi.org/10.3389/fspor.2022.850541>
6. Danielsen, J., Sandbakk, Ø., McGhie, D., Ettema, G.: Mechanical energy and propulsion mechanics in roller-skiing double-poling at increasing speeds. *PLOS ONE* (2021). <https://doi.org/10.1371/journal.pone.0255202>
7. Holmberg, H.-C., Lindinger, S., Stöggl, T., Björklund, G., Müller, E.: Contribution of the legs to double-poling performance in elite cross-country skiers. *Med. Sci. Sports Exerc.* **38**(10), 1853–1860 (2006). <https://doi.org/10.1249/01.mss.0000230121.83641.d1>
8. Lindinger, S., Holmberg, H.-C.: How do elite cross-country skiers adapt to different double poling frequencies at low to high speeds? *Eur. J. Appl. Physiol.* **111**, 1103–1119 (2011). <https://doi.org/10.1007/s00421-010-1736-8>
9. Pellegrini, B., Zoppirolli, C., Bortolan, L., Zamparo, P., Schena, F.: Gait models and mechanical energy in three cross-country skiing techniques. *J. Exp. Biol.* **217**(21), 3910–3918 (2014). <https://doi.org/10.1242/jeb.106740>
10. Stöggl, T.L., Holmberg, H.-C.: Double-poling biomechanics of elite cross-country skiers: Flat versus uphill terrain. *Med. Sci. Sports Exerc.* **48**(8), 1580–1589 (2016). <https://doi.org/10.1249/MSS.0000000000000943>
11. Sunde, A.: Stronger is better: The impact of upper body strength in double poling performance. *Front. Physiol.* **10**, 1091 (2019). <https://doi.org/10.3389/fphys.2019.01091>
12. Zoppirolli, C., Hébert-Losier, K., Holmberg, H.-C., Pellegrini, B.: Biomechanical determinants of cross-country skiing performance: A systematic review. *J. Sports Sci.* **38**, 2127–2148 (2020). <https://doi.org/10.1080/02640414.2020.1775375>
13. Zoppirolli, C., Holmberg, H.-C., Pellegrini, B., Quaglia, D., Bortolan, L., Schena, F.: The effectiveness of stretch-shortening cycling

- in upper-limb extensor muscles during elite cross-country skiing with the double-poling technique. *J. Electromyogr. Kinesiol.* **23**(6), 1512–1519 (2013). <https://doi.org/10.1016/j.jelekin.2013.08.013>
14. Zoppirolli, C., Pellegrini, B., Bortolan, L., Schena, F.: Energetics and biomechanics of double poling in regional and high-level cross-country skiers. *Eur. J. Appl. Physiol.* **115**, 969–979 (2015). <https://doi.org/10.1007/s00421-014-3078-4>
  15. Bowden, F.P., Hughes, T.P.: The mechanism of sliding on ice and snow. *Proc. R. Soc. Lond. A Math. Phys. Sci.* **172**, 280–298 (1939). <https://doi.org/10.1098/rspa.1939.0104>
  16. Bowden, F.P.: Friction on snow and ice. *Proc. R. Soc. Lond. A Math. Phys. Sci.* **217**, 462–478 (1953). <https://doi.org/10.1098/rspa.1953.0074>
  17. Hasler, M., Schindelwig, K., Mayr, B., Knoflach, Ch., Rohm, S., van Putten, J., Nachbauer, W.: A novel ski-snow tribometer and its precision. *Tribol. Lett.* (2016). <https://doi.org/10.1007/s11249-016-0719-2>
  18. Nachbauer, W., Kaps, P., Hasler, M., Mössner, M.: Friction between ski and snow. In: Braghin, F., Cheli, F., Maldifassi, S., Melzi, S., Sabbioni, E. (eds.) *The Engineering Approach Winter Sports*, pp. 17–32. Springer, New York (2016)
  19. Lehtovaara, A.: Kinetic friction between ski and snow. *Acta Polytech. Scand. Mech. Eng. Ser.* **93**, 52 (1989)
  20. Sandberg, J., Kalliorinne, K., Hindér, G., Holmberg, H.-C., Almqvist, A., Larsson, R.: A novel free-gliding ski tribometer for quantification of ski-snow friction with high precision. *Tribol. Lett.* (2023). <https://doi.org/10.1007/s11249-023-01781-w>
  21. Colbeck, S.C.: *A Review of the Processes that Control Snow Friction*. U.S. Army Corps of Engineers, Cold Regions Research and Engineering Laboratory (1992)
  22. Almqvist, A., Pellegrini, B., Lintzén, N., Emami, N., Holmberg, H.-C., Larsson, R.: A scientific perspective on reducing ski-snow friction to improve performance in Olympic cross-country skiing, the biathlon and Nordic combined. *Front. Sports Act. Living* **4**, 844883 (2022). <https://doi.org/10.3389/fspor.2022.844883>
  23. Müser, M.H., et al.: Meeting the contact-mechanics challenge. *Tribol. Lett.* **65**(4), 118 (2017). <https://doi.org/10.1007/s11249-017-0900-2>
  24. Vakis, A.I., et al.: Modeling and simulation in tribology across scales: An overview. *Tribol. Int.* **125**, 169–199 (2018). <https://doi.org/10.1016/j.triboint.2018.02.005>
  25. Mössner, M., Innerhofer, G., Schindelwig, K., Kaps, P., Schretter, H., Nachbauer, W.: Measurement of mechanical properties of snow for simulation of skiing. *J. Glaciol.* **59**(218), 1170–1178 (2013). <https://doi.org/10.3189/2013JG13J031>
  26. Mössner, M., Hasler, M., Nachbauer, W.: Calculation of the contact area between snow grains and ski base. *Tribol. Int.* **163**, 107183 (2021). <https://doi.org/10.1016/j.triboint.2021.107183>
  27. Theile, T., Szabo, D., Luthi, A., Rhyner, H., Schneebeli, M.: Mechanics of the ski-snow contact. *Tribol. Lett.* **36**, 223–231 (2009). <https://doi.org/10.1007/s11249-009-9476-9>
  28. Bäckström, M., Dahlen, L., Tinnsten, M.: Essential ski characteristics for cross-country skis performance (P251). *Eng. Sport* **7**, 543–549 (2008). [https://doi.org/10.1007/978-2-287-09413-2\\_66](https://doi.org/10.1007/978-2-287-09413-2_66)
  29. Breitschädel, F.: Effects of temperature change on cross-country ski characteristics. *Proc. Eng.* **2**(2), 2913–2918 (2010). <https://doi.org/10.1016/j.proeng.2010.04.087>
  30. Kalliorinne, K., Hindér, G., Sandberg, J., Larsson, R., Holmberg, H.-C., Almqvist, A.: The impact of cross-country skiers' tucking position on ski-camber profile, apparent contact area and load partitioning. *Proc. Inst. Mech. Eng. Part P: J. Sports Eng. Technol.* (2023). <https://doi.org/10.1177/17543371221141748>
  31. Walker, J., Questa, H., Raman, A., Ahmed, M., Mohammadpour, M., Bewsher, S.R., Offner, G.: Application of tribological artificial neural networks in machine elements. *Tribol. Lett.* (2023). <https://doi.org/10.1007/s11249-022-01673-5>
  32. Kalliorinne, K., Larsson, R., Pérez-RÃÁ, Æ'Ã fols, F., Liwicki, M., Almqvist, A.: Artificial neural network architecture for prediction of contact mechanical response. *Front. Mech. Eng.* **6**, 579825 (2021). <https://doi.org/10.3389/fmech.2020.579825>
  33. Kalliorinne, K., Sandberg, J., Hindér, G., Larsson, R., Holmberg, H.-C., Almqvist, A.: Characterisation of the contact between cross-country skis and snow: A macro-scale investigation of the apparent contact. *Lubricants* **10**(11), 279 (2022). <https://doi.org/10.3390/lubricants10110279>
  34. Stöggel, T., Karlöf, L.: Mechanical behaviour of cross-country ski racing poles during double poling. *Sports Biomech.* **12**(4), 365–380 (2013). <https://doi.org/10.1080/14763141.2013.840855>
  35. Jonsson, M., Welde, B., Stöggel, T.L.: Biomechanical differences in double poling between sexes and level of performance during a classical cross-country skiing competition. *J. Sports Sci.* **37**(14), 1582–1590 (2019). <https://doi.org/10.1080/02640414.2019.1577119>
  36. Torvik, P.-Ø., Sandbakk, Ø., van den Tillaar, R., Talsnes, R.K., Danielsen, J.: A comparison of double poling physiology and kinematics between long-distance and all-round cross-country skiers. *Front. Sports Act. Living* **4**, 849731 (2022). <https://doi.org/10.3389/fspor.2022.849731>
  37. Kalliorinne, K., Hindér, G., Sandberg, J., Larsson, R., Holmberg, H.-C., Almqvist, A.: Characterisation of the contact between cross-country skis and snow: On the multi-scale interaction between ski geometry and ski-base texture. *Lubricants* (2023). <https://doi.org/10.3390/lubricants11100427>
  38. Kalliorinne, K., Persson, B.N.J., Sandberg, J., Hindér, G., Larsson, R., Holmberg, H.-C., Almqvist, A.: Characterisation of the contact between cross-country skis and snow: A micro-scale study considering the ski-base texture. *Lubricants* (2023). <https://doi.org/10.3390/lubricants11050225>
  39. Almqvist, A., Sahlin, F., Larsson, R., Glavatskih, S.: On the dry elasto-plastic contact of nominally flat surfaces. *Tribol. Int.* **40**(4), 574–579 (2007). <https://doi.org/10.1016/j.triboint.2005.11.008>
  40. Sahlin, F., Larsson, R., Almqvist, A., Lugt, P.M., Marklund, P.: A mixed lubrication model incorporating measured surface topography—part 1: Theory of flow factors. *Proc. Inst. Mech. Eng. Part J: J. Eng. Tribol.* **2240**(4), 335–351 (2010). <https://doi.org/10.1243/13506501JET658>
  41. Wang, E., Fu, X., Han, H., Liu, X., Xiao, Y., Leng, Y.: Study on the mechanical properties of compacted snow under uniaxial compression and analysis of influencing factors. *Cold Reg. Sci. Technol.* **182**, 103215 (2021). <https://doi.org/10.1016/j.coldregions.2020.103215>
  42. Lintzén, N., Edeskär, T.: Uniaxial strength and deformation properties of machine-made snow. *J. Cold Reg. Eng.* **29**(4), 04014020 (2015). [https://doi.org/10.1061/\(ASCE\)CR.1943-5495.0000090](https://doi.org/10.1061/(ASCE)CR.1943-5495.0000090)
  43. Bahaloo, H., Gren, P., Casselgren, J., Forsberg, F., Sjö Dahl, M.: Capillary bridge in contact with ice particles can be related to the thin liquid film on ice. *J. Cold Reg. Eng.* (2024). <https://doi.org/10.1061/JCRGEI.CRENG-738>
  44. Lever, J.H., Asenath-Smith, E., Taylor, S., Lines, A.P.: Assessing the mechanisms thought to govern ice and snow friction and their interplay with substrate brittle behavior. *Front. Mech. Eng.* (2021). <https://doi.org/10.3389/fmech.2021.690425>
  45. Surkutwar, Y., Sandu, C., Untaroiu, C.: Review of modeling methods of compressed snow-tire interaction. *J. Terramech.* **105**, 27–40 (2023). <https://doi.org/10.1016/j.jterra.2022.10.004>
  46. Bahaloo, H., Forsberg, F., Casselgren, J., Lycksam, H., Sjö Dahl, M.: Mapping of density-dependent material properties of dry manufactured snow using  $\mu$ CT. *Appl. Phys. A* (2024). <https://doi.org/10.1007/s00339-023-07167-y>